DOI: 10.1002/adma.200501918

Multiwalled Carbon Nanotubes Beaded with ZnO Nanoparticles for Ultrafast Nonlinear Optical Switching**

By *Yanwu Zhu*, *Hendry Izaac Elim*, *Yong-Lim Foo*, *Ting Yu*, *Yanjiao Liu*, *Wei Ji*, *Jim-Yang Lee*, *Zexiang Shen*, *Andrew Thye-Shen Wee*, *John Thiam-Leong Thong*, and *Chorng-Haur Sow**

Nanoparticles—particles with sizes at the nanometer scale in all three dimensions—have attracted much attention because of their unique photonic, electronic, magnetic, and catalytic properties.[1] The assembly of isotropic nanoparticles onto one-dimensional (1D) architectures represents an important step towards the integration of nanoparticles into nanodevices.[2] In particular, nanoparticles of one material can be assembled on a 1D nanostructure of a different material to form unique and interesting hybrid nanomaterial systems.[3] Recently, carbon nanotubes (CNTs) have been used as templates or scaffolds for the hybrid assembly of nanoparticles.[4–10] Because of their great hardness and toughness, CNTs keep their morphology and structure even at high nanoparticle loadings. Using different methods, many types of metal and semiconductor nanoparticles, such as Au,[4] Ag,[5] Pt,[6] SnO_2,[7] TiO_2,[8] and CdSe,[9] have been assembled on CNTs. Recently, CNTs beaded with a variety of nanoparticles have been reported.[10–15] More importantly, some of these beaded CNT hybrid systems exhibit unique properties. For example, supercapacitance in a RuO_2/CNT composite,[16] diode-like rectification based on Co_3O_4-beaded CNTs,[11] and improved optical limiting from Au- and Ag-coated CNTs[15] have been demonstrated.

As an important wide-bandgap semiconductor (3.37 eV) with a large exciton binding energy (60 meV), ZnO has received widespread attention because of its excellent performance in electronics, optics, and photonics systems.[17] A range of 1D ZnO nanostructures have been fabricated.[17,18] ZnO nanoparticles and quantum dots have been synthesized by different methods,[19–22] and can also be assembled into 1D structures.[23] The two important building blocks in nanotechnology, ZnO nanoparticles and CNTs, have rarely been assembled as hybrid structures.[24–27] Kim and Sigmund[24] and Park and co-workers[25] have reported the coating of ZnO nanorods on CNTs by chemical vapor deposition (CVD) in a tube furnace. Gao and co-workers[26,27] have reported the deposition of ZnO particles on multiwalled CNTs (MWNTs) and their enhanced photocatalytic activity. The method includes decoration of MWNTs with sodium dodecyl sulfate (SDS) followed by reaction of zinc acetate with lithium hydroxide monohydrate in anhydrous ethanol. In hybrid systems, control of the particle size and interparticle distance is essential to their applications in electronic and photonic devices.[2] In addition, the functionalization of CNTs in order to anchor nanoparticles changes the surface properties of CNTs.[26,27] Hence, the potential of ZnO nanoparticles on CNT scaffolds for applications needs to be further investigated.

In this work, we report on a hybrid system of ZnO nanoparticles on MWNT scaffolds synthesized via a very simple and straightforward process. This involves the coating of pure Zn on as-grown, aligned MWNT films, followed by oxidization by simply heating the coated sample in air. After cooling, ZnO nanoparticles were found to have formed chain-like structures along the MWNTs, while the morphology of the aligned MWNTs remained unaltered. By directly changing the duration of the Zn coating step and thus the coating thickness, the average ZnO particle size and interparticle distance can be readily controlled. Based on this ZnO/MWNT hybrid system, an ultrafast nonlinear optical switching behavior has been demonstrated. Furthermore, three-photon adsorption of ZnO nanoparticles has been observed. Our results highlight opportunities for integrating CNTs with other functional oxide nanoparticles via a simple method, and for exploring the collective properties of nanoparticles/CNT hybrid materials.

[*] Prof. C. H. Sow, Y. Zhu, Dr. T. Yu, Y. Liu, Prof. W. Ji, Prof. A. T. S. Wee
Department of Physics
National University of Singapore (NUS)
2 Science Drive 3, 117542 (Singapore)
E-mail: physowch@nus.edu.sg
Prof. C. H. Sow, Y. Zhu, Prof. A. T. S. Wee, Prof. J. T. L. Thong
National University of Singapore (NUS)
Nanoscience and Nanotechnology Initiative
S13, 2 Science Drive 3, 117542 (Singapore)
H. I. Elim, Prof. J.-Y. Lee
Department of Chemistry and Biomolecular Engineering
National University of Singapore (NUS)
4 Engineering Drive 4, 117576 (Singapore)
Dr. Y. L. Foo
Institute of Materials Research and Engineering
3 Research Link, 117602 (Singapore)
Prof. Z. Shen
School of Physical and Mathematical Sciences
Nanyang Technological University
1 Nanyang Walk, 637616 (Singapore)
Prof. J. T. L. Thong
Department of Electrical and Computer Engineering
National University of Singapore (NUS)
4 Engineering Drive 3, 117576 (Singapore)

[**] The authors acknowledge support from the NUS Academic Research Fund. Y. Zhu thanks K. C. Chin for his help on sputtering, and J. L. Kwek, W. Y. Kan, and X. Y. Leong for their help on the morphology characterization. T. Yu acknowledges the support of the Singapore Millennium Foundation.

ADVANCED MATERIALS

Moreover, it is expected that the larger specific surface area of ZnO nanoparticles on CNT forests would further enhance the performance of ZnO as a biological catalyst and gas sensor.

The typical morphologies of the as-grown CNTs and of the CNTs beaded with ZnO nanoparticles have been analyzed by scanning electron microscopy (SEM). Figure 1 shows the general surface morphology of as-grown MWNTs with a diameter of 15–40 nm and a length of about 10 μm deposited on a Si substrate. After heating Zn-coated CNTs at 400 °C in ambient conditions for two hours, the original smooth MWNTs were decorated by ZnO nanoparticles, forming chain-like structures. Figures 2a,c,e show images of these structures corresponding to a Zn-coating step duration of 1, 3, and 5 min, respectively. Calibration showed that the deposition rate of Zn on the upper part of aligned CNTs was about 10 nm min^{-1}. Figures 2b,d,f show the diameter distributions of ZnO nanoparticles for each coating duration. From Figure 2, we can see that with the increase in the Zn-coating thickness the average diameter of ZnO nanoparticles increases from 19.2 nm to 26.2 and 36.6 nm. At the same time, the sample coated for 3 min shows the narrowest size distribution, about 3.5 nm. For each case, the size distribution of ZnO nanoparticles roughly follows a Gaussian profile, as shown in the fitting curves in Figures 2b,d,f. On the other hand, with the increase in coating thickness, the average distance between particles is reduced. For the ZnO-beaded MWNTs with a coating time of 1 min, there is a narrow gap between adjacent nanoparticles. For MWNTs coated with Zn for 3 min, almost all particles are connected. After coating for 5 min, the particles begin to overlap and aggregate. Coating for 7 min has also been attempted, but then all particles piled together and few isolated individual particles could be distinguished. Such controllable interaction between adjacent nanoparticles along one dimension is very important to the collective behavior in nanoparticle assemblies.[28]

Resonant micro-Raman spectroscopy and photoluminescence (PL) spectroscopy using a He–Cd laser (325 nm,

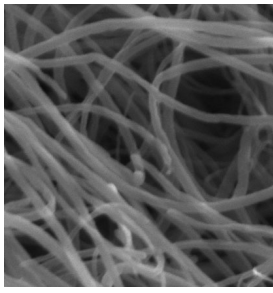

Figure 1. Typical SEM image of the as-grown MWNTs.

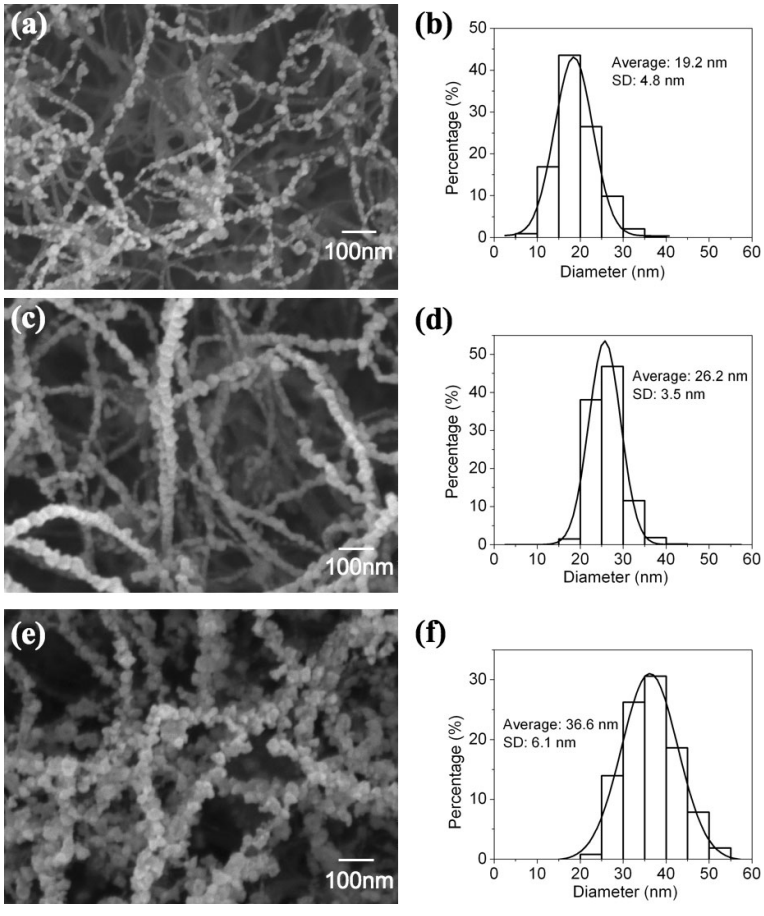

Figure 2. Typical SEM images of ZnO-beaded MWNTs with coating times of a) 1 min, c) 3 min, and e) 5 min; b,d,f) corresponding diameter distributions of ZnO nanoparticles in samples (a,c,e), respectively. Solid lines in (b,d,f) represent the Gaussian fitting curves. SD = standard deviation.

40 mW) under back-scattering geometry have been employed to characterize the as-grown and ZnO-beaded MWNTs. The results are shown in Figures 3a,b, respectively. From Figure 3a, we can see that with the increase in the Zn-coating thickness, three additional peaks, besides the original D (dis-

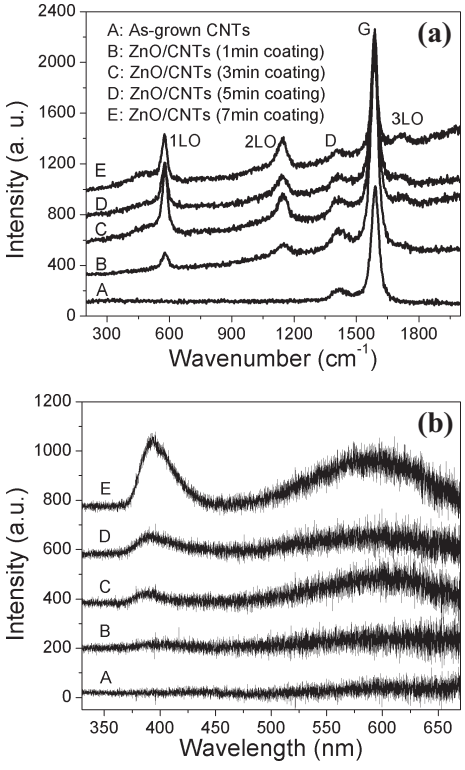

Figure 3. a) Resonant micro-Raman spectra and b) PL spectra from as-grown MWNTs and ZnO-beaded MWNTs with different coating durations. LO: longitudinal optical.

ordered carbon, at about 1350 cm^{-1}) and G (sp^2 carbon, at about 1580 cm^{-1}) bands of MWNTs, begin to appear at about 574, 1148, and 1720 cm^{-1}. The three peaks are attributed to the multiples of 1-longitudinal optical (1LO) phonons of ZnO, which are often observed in ZnO bulk crystals,[29] single-crystalline ZnO nanowires,[30] and some high-quality ZnO nanoparticles.[21,31–33] We have also noticed that, in the Raman spectra of ZnO, the full width at half maximum (FWHM) of the 1LO peak varies between 31 and 33 cm^{-1} for samples coated for 3, 5, and 7 min, and increases to 40 cm^{-1} for the sample coated for 1 min. Such broadening of Raman peaks in ZnO nanoparticles compared with those of ZnO crystals[34] could be a result of the confinement of optical phonons, oxygen deficiencies, and residual stress in the ZnO nanoparticles.[30,35,36] However, no remarkable red-shift of the peak position is found, compared to previous reports.[32,33,35] In Figure 3b, for the sample coated with Zn for 1 min, no obvious PL peak is observed because of the low concentration of ZnO nanoparticles and limited sensitivity of our PL detector. However, in samples coated for 3, 5, and 7 min, one blue emission peak and one broad yellow–green band are detected. The blue peak is associated with the recombination of free excitons in ZnO.[22,25,37] It can be seen that the intensity of the blue peak increases with the ZnO content, and that its position shifts slightly from 386 nm to 390 and 394 nm upon increasing the coating duration from 3 min to 5 and 7 min. Such a red-shift with particle size is believed to arise from the quantum-confinement-induced enhancement of the energy gap, which has been reported in ZnO nanocrystallites with 20–60 nm particle sizes.[21,37–39] The broad yellow–green band is generally attributed to the oxygen vacancies and/or interstitial Zn ions in the ZnO lattice.[22,25,36,37] Furthermore, it is worth noting that in our case the ratio of blue-band intensity to yellow–green-band intensity increases with the particle size. This observation is similar to the results obtained for ZnO nanowires[40,41] and quantum dots,[42] suggesting that surface recombination may also play an important role in the broad yellow–green emission of this ZnO/MWNT hybrid system.[40]

To further explore the microstructure of MWNTs beaded with ZnO nanoparticles, transmission electron microscopy (TEM) and high-resolution TEM (HRTEM) have been carried out. Figures 4a,b show typical TEM images of the samples coated with Zn for 3 min and 5 min, respectively. It can be

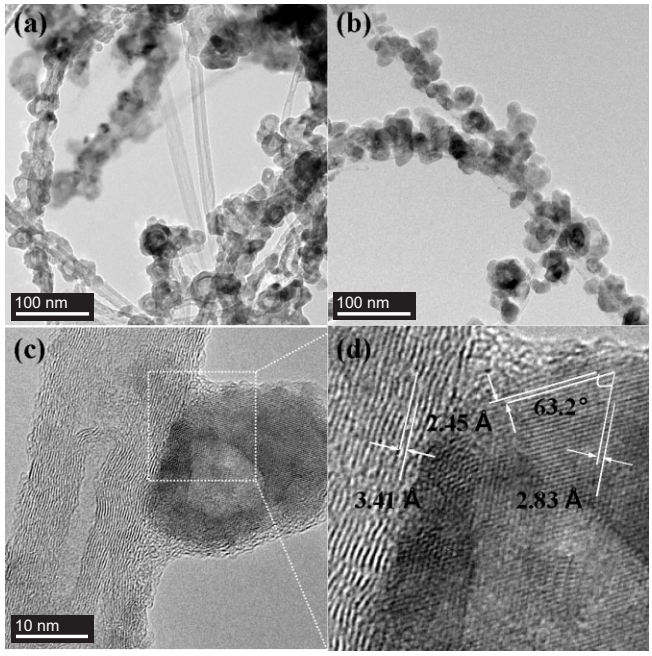

Figure 4. Typical TEM images of ZnO-beaded MWNTs with Zn-coating durations of a) 3 min and b) 5 min. c) HRTEM image of (a) showing a hollow particle on a MWNT. d) Magnified HRTEM image, taken from the square area in (c).

seen that in the 3 min coating step, hollow ZnO beads are formed along the MWNTs, while, when coated for 5 min, most of the particles are solid. Such hollow beads have also been found in the products from the sample coated with Zn for 1 min. As shown in Figure 4a, some cavities in the hollow beads seem to have a polyhedral shape, although the particles themselves do not have a regular shape—in contrast to the

ADVANCED MATERIALS

ZnO submicrometer-sized hollow beads reported in the literature,[18] in which the polyhedral ZnO beads have spherical cavities. Figure 4c shows an HRTEM image of a ZnO nanoparticle on a MWNT coated for 3 min. The intact MWNT structure and crystalline fringes of ZnO nanoparticles are clearly observed. There is a thin amorphous layer surrounding the whole particle and connecting it to the wall of the MWNT at the same time. Such compact connection between the MWNT and the ZnO nanoparticle could be due to the good wettability of melted Zn on the surface of CNTs.[24] More details can be seen by enlarging the square highlighted in Figure 4c, shown in Figure 4d. From the figure, the spacing between adjacent walls of the MWNT has been determined to be 3.41 Å, a value similar to the layer spacing in graphite. For the nanoparticle, two lattice spacings of 2.45 Å and 2.83 Å were obtained. In addition, an interfacial angle of 63.2° has also been measured. These results are consistent with the following collections of hexagonal ZnO interplanar distances:[43] {011}‖{100}, {011}‖{1–10} and {1–11}‖{100}. Although the {100} or {1–10} faces of ZnO nanoparticles are roughly parallel to the wall of the MWNT, the tubular CNT wall makes it difficult to grow epitaxially the ZnO nanoparticle, which has a non-layered structure. Thus, this region is expected to be highly defective in order to release a large mount of strain at the interface.[44]

The chemical composition of the ZnO/MWNT hybrid products was further confirmed by X-ray photoelectron spectroscopy (XPS). Figure 5a shows the C1s spectra from as-grown and ZnO-beaded MWNTs. After beading the MWNTs with ZnO nanoparticles, the C1s peak intensity is significantly decreased, suggesting that CNTs are covered by nanoparticles. The peak positions also shift to higher binding energies with increasing duration of the Zn-coating step. To clarify the details, the Gaussian decomposition of the peaks of as-grown CNTs and ZnO-beaded CNTs (coated for 3 min) is shown in Figure 5b. For the as-grown CNTs, the spectrum consists of at least two components. The peak at about 284.6 eV is attributed to the graphitic carbon on the walls of the MWNTs, and the other peak, located at about 285.7 eV, is due to C–O bonds that may be attributed to surface hydroxyl groups.[11,45] After beading with ZnO nanoparticles, the spectrum shows three peaks. Although the peak at 285.0 eV has a higher binding energy, it is still assigned to C–C binding.[46,47] Also, the peaks at about 286.2 eV and 287.2 eV are considered to originate from the C–OH and C=O groups, respectively.[48–50] At the same time, the intensity of the O1s spectra increases, and the peaks tend to shift to lower binding energies after beading with ZnO nanoparticles, as shown in Figure 5c. Such peak shifts are due to the fact that both the oxygen in ZnO (530.6–531 eV)[21,51] and in C=O (about 531.3 eV) have lower binding energies than the oxygen in C–O (about 533 eV).[52,53] Figure 5d shows that typical Zn2p spectra are observed from ZnO-beaded CNT samples and the peak positions remain constant. No Zn–C bonding has been found. These XPS spectra clearly demonstrate the successful beading of ZnO on CNTs and the formation of strong covalent single and double bonds between carbon and oxygen atoms, which is consistent with other metal oxide/CNT composite materials.[45,46]

Using femtosecond laser pulses at a wavelength of 780 nm, we have observed ultrafast absorptive nonlinearities in films of MWNTs beaded with ZnO nanoparticles on quartz substrates. To minimize the average power and reduce accumulative thermal effects, 220 fs laser pulses at a 1 kHz repetition rate were

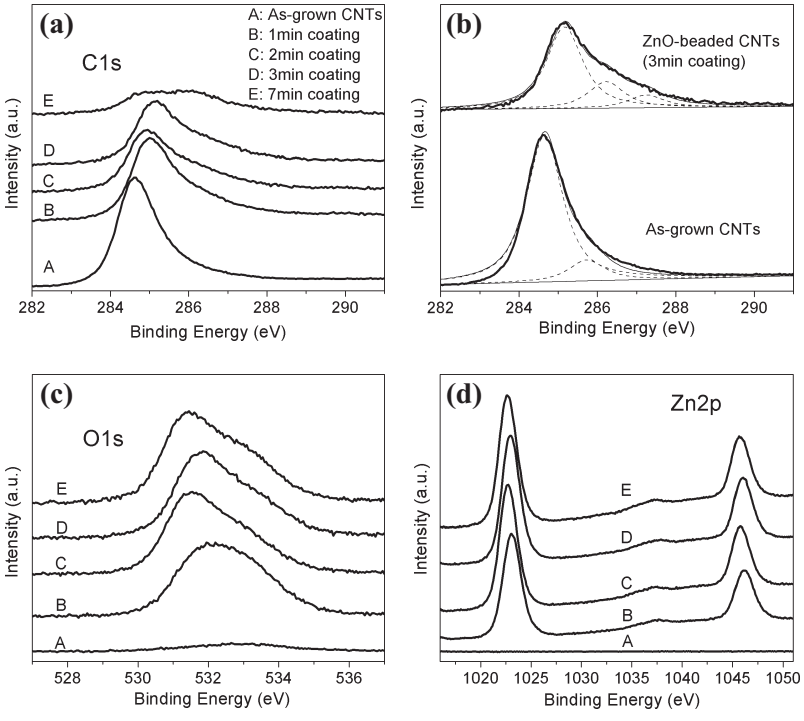

Figure 5. a) XPS C1s spectra from as-grown and ZnO-beaded MWNTs. b) Gaussian decomposition of C1s spectra of as-grown MWNTs (bottom) and ZnO-beaded MWNTs (coated with Zn for 3 min, top). c) O1s spectra. d) Zn2p spectra.

employed. The laser pulses were focused onto the samples with a minimum beam waist of about 15 μm. The incident and transmitted laser powers were monitored as the samples were moved (or z-scanned) along the propagation direction of the laser pulses. Figure 6a displays the typical open-aperture z-scans, showing negative signs for the absorptive nonlinearity. The z-scan curve of as-grown MWNTs shows a typical signal

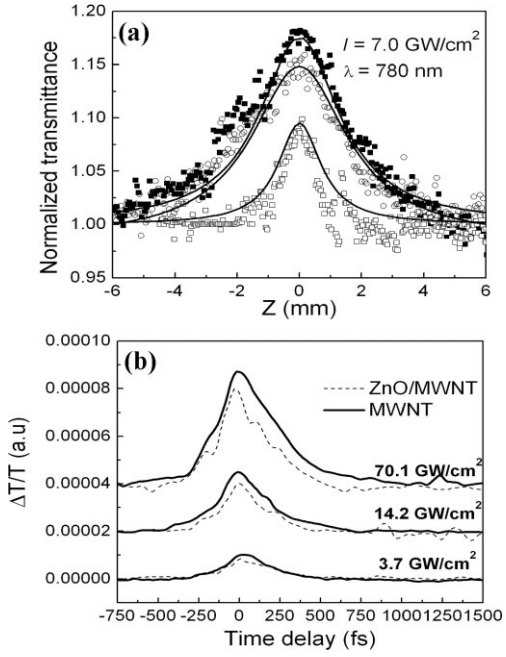

Figure 6. a) Open-aperture z-scans of the as-grown MWNTs (filled squares) and ZnO-beaded MWNTs (coated with Zn for 1 min) (open circles) and 5 min (open squares), recorded with an irradiance of 7.0 GW cm^{-2}. The solid lines are the best-fit curves calculated using the z-scan theory [56]. b) Degenerate 220 fs time-resolved pump–probe measurements of the as-grown and ZnO-beaded MWNTs (coated with Zn for 5 min) performed at 780 nm with different pump irradiances. The top curves are shifted vertically for clear presentation.

for saturable absorption, consistent with our previous report.[54] On the other hand, the transmittance from ZnO/MWNTs (coated for 1 min) is only slightly smaller than that from as-grown MWNTs. However, for the sample coated for 5 min, the normalized transmittance is significantly reduced. Such a reduction is believed to be induced by three-photon absorption in the presence of ZnO nanoparticles. With the total energy of three photons (3×1.59 eV), a valence-band electron can be excited to the conduction band in ZnO ($E_g = 3.37$ eV for bulk ZnO, where E_g is the bandgap energy). Such a nonlinear process gives rise to a positive contribution to the nonlinear absorption, in contrast to the contribution to the saturable absorption. The details of three-photon absorption in ZnO nanoparticles can be found in our previous work,[55] in which only positive absorption signals have been observed. Here, due to the saturable absorption of MWNTs, the resultant nonlinear absorption is the interplay between the three-photon absorption in ZnO nanoparticles and the saturable absorption in MWNTs. Such an interplay provides an effective way to control the nonlinear response by changing the concentration of the ZnO nanoparticles in our ZnO/MWNTs hybrid system.

We assume that the observed absorptive nonlinearity can be described by $\Delta a = a_2 I$, where a_2 is the effective third-order nonlinear absorption coefficient and I is the light irradiance. The a_2 value can be extracted from the best fit between the data and the z-scan theory.[56] At 780 nm, $a_2 = -30$ cm GW^{-1} (or $\mathrm{Im}\chi^{(3)} = -1.7 \times 10^{-11}$ esu ($\chi^{(3)}$ (SI units) $= 4\pi/9 \times 10^{-8} \chi^{(3)}$ (esu)); $\chi^{(3)}$: the imaginary part of the third- order nonlinear susceptibility) can be obtained for the as-grown MWNT film, while the a_2 (or $\mathrm{Im}\chi^{(3)}$) for ZnO-beaded MWNTs (coated for 5 min) is –21 cm GW^{-1} (or $\mathrm{Im}\chi^{(3)} = -1.1 \times 10^{-11}$ esu). Here, $\mathrm{Im}\chi^{(3)}$ represents the imaginary part of the third-order nonlinear adsorption susceptibility. By comparison, a value of 8.3×10^{-13} esu at 800 nm was observed for $|\chi^{(3)}|$ in carbon nanoparticles embedded in sol–gel SiO_2 glass.[57] For a single-walled CNT (SWNT) solution at a concentration of 0.33 mg mL^{-1}, it has been reported to be 4×10^{-13} esu at 820 nm.[58] Our larger value of $|\chi^{(3)}|$ is attributed to the high concentration of MWNTs and ZnO nanoparticles packed as a thin film.

To evaluate the recovery time of the observed nonlinearities and to gain an insight into the underlying mechanism, a degenerate pump–probe experiment was conducted with 220 fs, 780 nm laser pulses. Figure 6b displays the transient absorption signals of both as-grown MWNTs and ZnO-beaded MWNTs (coated for 5 min) at the same wavelength. In this experiment, the pump irradiance was varied from 3.7 GW cm^{-2} to 70.1 GW cm^{-2}, and a saturable absorption (SA) effect was observable. The results in Figure 6b confirm the SA processes measured using z-scans as depicted in Figure 6a. In these pump–probe studies, all the signals from both MWNTs and ZnO-beaded MWNTs show an effectively negative nonlinear absorption predominantly due to photoinduced bleaching. At a very high irradiance, both MWNTs and ZnO-beaded MWNTs reveal clear saturable absorption or optical-induced transparency. In this saturation regime, most of the carrier states are filled, and, thus, the sample absorption is completely quenched. A similar observation has been made for semiconducting SWNTs by Ostojic et al.[59] Such saturation in SWNTs was observed at a low fluence of 1 mJ cm^{-2} (~7 GW cm^{-2}). In our case, such a process may involve the carrier shift between ZnO nanoparticles and CNTs, a possibility that deserves further investigation. The large and ultrafast saturable absorption in ZnO-beaded MWNTs suggests that the samples can be used as saturable absorber devices. These devices can offer a potentially simple and cost-effective solution for passive optical regeneration, error-free transmission distances for periodically amplified optical transmission systems, laser-mode locking based on a saturable absorber, and high noise-suppression capability, as reported by Set et al.[60] and Yamashita et al.[61] Furthermore, combining the three-photon absorption properties of ZnO with the saturable absorption properties of CNTs to yield ZnO/MWNTs hybrid materials would also find important applications in future multifunctional nanodevices.

ADVANCED MATERIALS

Experimental

Aligned MWNTs were grown on silicon substrates coated with iron nanoparticles using plasma-enhanced chemical vapor deposition (PECVD) [62]. The iron nanoparticle catalyst was sputtered onto the substrate by radio-frequency (RF) sputtering. After that, the as-grown MWNTs were placed into an RF plasma-assisted sputtering system (Denton Discovery-18) to be sputtered with a Zn film at room temperature (20 °C). The details can be found in our previous report [63]. Ar plasma at a power of about 100 W was induced to bombard a pure Zn (99.9%, Aldrich) target. The deposition duration varied from 1 to 7 min. Subsequently, as-sputtered samples were put onto a hot plate and heated at 400 °C in ambient conditions for 2 h. After cooling, the as-grown products were characterized by SEM (JEOL JSM-6400F), TEM (Philips CM300, 300kV), micro-Raman/PL spectroscopy (Renishaw), and XPS (ESCA MK II; Mg source). For the measurement of nonlinear optical performance, the MWNTs were grown on quartz substrates and then beaded with ZnO nanoparticles by following the same procedure. The laser pulses were generated by a mode-locked Ti:sapphire laser (Quantronix, IMRA) that seeded a Ti:sapphire regenerative amplifier (Quantronix, Titan).

Received: September 12, 2005
Final version: November 22, 2005

[1] A. P. Alivisatos, *Science* **1996**, *271*, 933.
[2] Z. Tang, N. A. Kotov, *Adv. Mater.* **2005**, *17*, 951.
[3] E. C. Walter, B. J. Murray, F. Favier, R. M. Penner, *Adv. Mater.* **2003**, *15*, 396.
[4] S. Fullam, D. Cottel, H. Rensmo, D. Fitzmaurice, *Adv. Mater.* **2000**, *12*, 1430.
[5] Y. P. Sun, W. Huang, Y. Lin, K. Fu, A. Kitaygorodskiy, L. A. Riddle, Y. J. Yu, D. L. Carroll, *Chem. Mater.* **2001**, *13*, 2864.
[6] M. Endo, Y. A. Kim, M. Ezaka, K. Osada, T. Yanagisawa, T. Hayashi, M. Terrones, M. S. Dresselhaus, *Nano Lett.* **2003**, *3*, 723.
[7] W. Q. Han, A. Zettl, *Nano Lett.* **2003**, *3*, 681.
[8] X. Li, J. Niu, J. Zhang, H. Li, Z. Liu, *J. Phys. Chem. B* **2003**, *107*, 2453.
[9] F. E. Osterloh, J. S. Martino, H. Hiramatsu, D. P. Hewitt, *Nano Lett.* **2003**, *3*, 125.
[10] W. A. de Heer, P. Poncharal, C. Berger, J. Gezo, Z. Song, J. Bettini, D. Ugarte, *Science* **2005**, *307*, 907.
[11] L. Fu, Z. Liu, Y. Liu, B. Han, P. Hu, L. Cao, D. Zhu, *Adv. Mater.* **2005**, *17*, 217.
[12] X. Xiao, J. W. Elam, S. Trasobares, O. Auciello, J. A. Carlisle, *Adv. Mater.* **2005**, *17*, 1496.
[13] B. M. Quinn, C. Dekker, S. G. Lemay, *J. Am. Chem. Soc.* **2005**, *127*, 6146.
[14] S. Agrawal, A. Kumar, M. J. Frederick, G. Ramanath, *Small* **2005**, *1*, 823.
[15] K. C. Chin, A. Gohel, W. Z. Chen, H. I. Elim, W. Ji, G. L. Chong, C. H. Sow, A. T. S. Wee, *Chem. Phys. Lett.* **2005**, *409*, 85.
[16] J. S. Ye, H. F. Cui, X. Liu, T. M. Lim, W. D. Zhang, F. S. Sheu, *Small* **2005**, *1*, 560.
[17] Z. L. Wang, *J. Phys.: Condens. Matter* **2004**, *16*, R829.
[18] Z. L. Wang, *Mater. Today* **2004**, *8(6)*, 26.
[19] Z. Y. Jiang, Z. X. Xie, X. H. Zhang, S. C. Lin, T. Xu, S. Y. Xie, R. B. Huang, L. S. Zheng, *Adv. Mater.* **2004**, *16*, 904.
[20] L. Mädler, W. J. Stark, S. E. Pratsinis, *J. Appl. Phys.* **2002**, *92*, 6537.
[21] Z. Wang, H. Zhang, L. Zhang, J. Yuan, S. Yan, C. Wang, *Nanotechnology* **2003**, *14*, 11.
[22] J. Joo, S. G. Kwon, J. H. Yu, T. Hyeon, *Adv. Mater.* **2005**, *17*, 1837.
[23] C. Pacholski, A. Kornowski, H. Weller, *Angew. Chem. Int. Ed.* **2002**, *41*, 1188.
[24] H. Kim, W. Sigmund, *Appl. Phys. Lett.* **2002**, *81*, 2085.
[25] S. Y. Bae, H. W. Seo, H. C. Choi, J. Park, J. Park, *J. Phys. Chem. B* **2004**, *108*, 12 318.
[26] J. Sun, L. Gao, M. Iwasa, *Chem. Commun.* **2004**, 832.
[27] L. Jiang, L. Gao, *Mater. Chem. Phys.* **2005**, *91*, 313.
[28] L. Zhao, K. L. Kelly, G. C. Schatz, *J. Phys. Chem. B* **2003**, *107*, 7343.
[29] J. F. Scott, *Phys. Rev.* **1970**, *2*, 1209.
[30] H. T. Ng, B. Chen, J. Li, J. Han, M. Meyyappan, J. Wu, S. X. Li, E. E. Haller, *Appl. Phys. Lett.* **2003**, *82*, 2023.
[31] J. G. Ma, Y. C. Liu, C. L. Shao, J. Y. Zhang, Y. M. Lu, D. Z. Shen, X. W. Fan, *Phys. Rev. B: Condens. Matter Mater. Phys.* **2005**, *71*, 125 430.
[32] K. A. Alim, V. A. Fonoberov, A. A. Balandin, *Appl. Phys. Lett.* **2005**, *86*, 53 103.
[33] K. A. Alim, V. A. Fonoberov, M. Shamsa, A. A. Balandin, *J. Appl. Phys.* **2005**, *97*, 124 313.
[34] T. C. Damen, S. P. S. Porto, B. Tell, *Phys. Rev.* **1966**, *142*, 570.
[35] C. Geng, Y. Jiang, Y. Yao, X. Meng, J. A. Zapien, C. S. Lee, Y. Lifshitz, S. T. Lee, *Adv. Funct. Mater.* **2004**, *14*, 589.
[36] Y. Du, M. S. Zhang, J. Hong, Y. Shen, Q. Chen, Z. Yin, *Appl. Phys. A: Mater. Sci. Process.* **2003**, *76*, 171.
[37] S. Cho, J. Ma, Y. Kim, G. K. L. Wong, J. B. Ketterson, *Appl. Phys. Lett.* **1999**, *75*, 2761.
[38] V. Srikant, D. R. Clarke, *J. Mater. Res.* **1997**, *12*, 1425.
[39] T. Yatsui, T. Kawazoe, T. Shimizu, Y. Yamamoto, M. Ueda, M. Kourogi, M. Ohtsu, G. H. Lee, *Appl. Phys. Lett.* **2002**, *80*, 1444.
[40] M. H. Huang, Y. Wu, H. Feick, N. Tran, E. Weber, P. Yang, *Adv. Mater.* **2001**, *13*, 113.
[41] I. Shalish, H. Temkin, V. Narayanamurti, *Phys. Rev. B: Condens. Matter Mater. Phys.* **2004**, *69*, 245 401.
[42] A. van Dijken, J. Makkinje, A. Meijerink, *J. Lumin.* **2001**, *92*, 323.
[43] Joint Committee on Powder Diffraction Standards (JCPDS) Card No. 80-0075.
[44] L. Pan, K. K. Lew, J. M. Redwing, E. C. Dickey, *Nano Lett.* **2005**, *5*, 1081.
[45] Y. Shan, L. Gao, *Nanotechnology* **2005**, *16*, 625.
[46] L. Chen, B. L. Zhang, M. Z. Qu, Z. L. Yu, *Powder Technol.* **2005**, *154*, 70.
[47] A. M. Bond, W. Miao, C. L. Raston, *Langmuir* **2000**, *16*, 6004.
[48] N. I. Kovtyukhova, T. E. Mallouk, L. Pan, E. C. Dickey, *J. Am. Chem. Soc.* **2003**, *125*, 9761.
[49] H. Ago, T. Kugler, F. Cacialli, W. R. Salaneck, M. S. P. Shaffer, A. H. Windle, R. H. Friend, *J. Phys. Chem. B* **1999**, *103*, 8116.
[50] M. Liu, Y. Yang, T. Zhu, Z. Liu, *Carbon* **2005**, *43*, 1470.
[51] J. D. Ye, S. L. Gu, F. Qin, S. M. Zhu, S. M. Liu, X. Zhou, W. Liu, L. Q. Hu, R. Zhang, Y. Shi, Y. D. Zheng, Y. D. Ye, *Appl. Phys. A: Mater. Sci. Process.* **2005**, *81*, 809.
[52] Y. Xing, L. Li, C. C. Chusuei, R. V. Hull, *Langmuir* **2005**, *21*, 4185.
[53] M. T. Martinez, M. A. Callejas, A. M. Benito, M. Cochet, T. Seeger, A. Anson, J. Schreiber, C. Gordon, C. Marhic, O. Chauvet, J. L. G. Fierro, W. K. Maser, *Carbon* **2003**, *41*, 2247.
[54] H. I. Elim, W. Ji, G. H. Ma, K. Y. Lim, C. H. Sow, C. H. A. Huan, *Appl. Phys. Lett.* **2004**, *85*, 1799.
[55] W. Ji, Y. Qu, J. Mi, Y. Zheng, J. Y. Ying, *Chin. Opt. Lett.* **2005**, *3*, 1671.
[56] M. Sheik-Bahae, A. A. Said, T. Wei, D. J. Hagan, E. W. Van Stryland, *IEEE J. Quantum Electron.* **1990**, *26*, 760.
[57] D. Li, Y. Liu, H. Yang, S. Qian, *Appl. Phys. Lett.* **2002**, *81*, 2088.
[58] S. Wang, W. Huang, H. Yang, Q. Gong, Z. Shi, X. Zhou, D. Qiang, Z. Gu, *Chem. Phys. Lett.* **2000**, *320*, 411.
[59] G. N. Ostojic, S. Zaric, J. Kono, M. S. Strano, V. C. Moore, R. H. Huage, R. E. Smalley, *Phys. Rev. Lett.* **2004**, *92*, 117 402.
[60] S. Y. Set, H. Yaguchi, Y. Tanaka, M. Jablonski, *J. Lightwave Technol.* **2004**, *22*, 51.
[61] S. Yamashita, Y. Inoue, S. Maruyama, Y. Murakami, H. Yaguchi, M. Jablonski, S. Y. Set, *Opt. Lett.* **2004**, *29*, 1581.
[62] Y. H. Wang, J. Lin, C. H. A. Huan, G. S. Chen, *Appl. Phys. Lett.* **2001**, *79*, 680.
[63] Y. W. Zhu, T. Yu, C. H. Sow, Y. J. Liu, A. T. S. Wee, X. J. Xu, C. T. Lim, J. T. L. Thong, *Appl. Phys. Lett.* **2005**, *87*, 023 103.

